FN-318
2251.0

Fermilab

NEUTRINO BEAMS IN THE ENERGY RANGE OF 20 TEV *

S.Mori
Fermilab
November 8, 1979

I. Introduction

The conceptual design of a narrow-band dichromatic beam has been described in the Proceedings of the previous meeting and will not be discussed here. I will discuss wide-band neutrino beams and beam dump neutrino beams.

II. Wide-Band Muon Neutrino Beams

One of the most important questions in designing neutrino beams is how to shield neutrino detectors, particularly bubble chambers, from muon backgrounds. Figures 1 and 2 show computed dE/dx and ranges of muons in soil, iron and uranium in the muon energy range above 1 TeV by G.Koizumi[1]. Energy losses due to radiation processes (pair production and bremsstrahlung) become very large for high Z elements in this energy range. The solid curves correspond to the case where energy losses due to atomic collisions and pair productions are included and the dashed curves correspond to the case where energy losses due to bremsstrahlung are added. The distribution of the fractional energy loss for the bremsstrahlung process is nearly flat and the average energy loss for this process is very large compared to the other two processes[2]. Therefore, the bremsstrahlung process causes a large struggling in the absorption range and should not be included in the muon shield calculations.

The muon shield length which includes muon detector stations for flux monitoring can be 2 km or less without using any active magnetic shielding. It will be very effective to use high Z material near the beam axis at the upstream end of the shield. A muon shield of 2 km for the wide-band beams was assumed in the present study.

A Monte Carlo program was used to compute neutrino fluxes. Figure 3 shows computed neutrino fluxes for various decay path lengths from 2 km to 20 km at the incident proton energy of 20 TeV. Wang's formula[3] was used for pion and kaon production. The detector radius was 0.5m. No focussing device

was used (bare target beam). A decay path length of 4 km appears roughly optimum in the medium neutrino energy range below 10 TeV. The longer decay path is favorable for high energy neutrino beams, however, there seems to be essentially no gain by having a decay path longer than 10 km for the bare target beam with a detector radius of 0.5 m.

The angular dependence of the neutrino beam intensity is shown in Figure 4 for the decay path lengths of 4 km and 10 km and detector radial intervals, 0 to .25 m, 0.5 to 0.75 m, and 1.0 to 1.25 m. For a detector with a small radius (~ 0.25 m) the 4 km long decay path can provide a good neutrino flux even above 10 TeV. Figure 5 shows neutrino fluxes at incident proton energies of 1, 5, 10, and 20 TeV for the decay path length of 4 km. Table I gives integrated event rates for a detector with a fiducial volume of 100 tons and 10^{13} incident protons. The detector radius was 0.5 m. The total cross section of ν_μ nucleon interactions was assumed to be $0.65 \cdot E_\nu$ (in GeV) x 10^{-38} cm^2.

For some experiments it might be desirable to suppress low energy neutrinos because of high event rates. This can be achieved by a "dog-leg" arrangement of two sets of dipole magnets[4], or a triplet focussing of conventional quadrupole magnets[5], or horns with parabolic inner conductors[6]. Figure 6 shows neutrino fluxes as a function of the aperture of a beam collimator in a dog-leg arrangement. Enriched neutrino and antineutrino beams can be obtained by closing one side of the collimator. A beam dump for the primary proton beam must be installed upstream of the collimator for the antineutrino beam. Although details have not been studied, sign selection capabilities by any horn system will be very limited at high energies since most high energy particles are produced preferentially in the very forward direction of the horn inner conductor "neck" area.

For bubble chambers it is absolutely necessary to have the capability of multi-fast pulse extraction as discussed in the Fermilab 1976 Summer Studies[7]. It may also require a special shield arrangement to limit the number of muons produced from neutrino interactions in the shield material upstream of the bubble chambers.

Finally it must be noted that the arrangement of the decay pipe and muon shield for the wide-band beam is totally different from that for the narrow-band beam.

III. Neutrino Beams From a Beam Dump

Neutrino beam intensities from short-lived sources in a beam dump are roughly proportional to the square of the distance between the dump and the neutrino detector. Therefore, it is important to make this distance as short as possible. In the present calculations the distance was assumed to be 1 km. A combination of passive shield of high Z material and active magnetic shield may allow us to have even a shorter distance.

Fluxes of τ neutrinos and antineutrinos from a beam dump were calculated using a Monte Carlo program. The following assumptions were made in the calculations:

1. τ neutrinos, ν_τ, were produced from the F^+ meson decay, $F^+ \to \tau^+\nu_\tau$ (B.R. = 3%), and the τ^- decay, $\tau^- \to \ell^-\bar{\nu}_\ell\nu_\tau$ (B.R. = 36%), $\pi^-\nu_\tau$ (B.R. = 10%) and $\rho^-\nu_\tau$ (B.R. = 20%), where the ℓ is the e or μ. The τ^- is the decay product of the F^-. Conversely, τ antineutrinos, $\bar{\nu}_\tau$, were produced from the F^- and τ^+ decays. The mass of the F was 2.06 GeV.
2. Other decay modes of the τ (34%) were not included.
3. The helicity state of the τ from the F decay was not taken into account in the τ decay.
4. The energy spectrum of the ν_τ from $\tau^- \to \ell^-\bar{\nu}_\ell\nu_\tau$ had the form of $(3-2\varepsilon)\,\varepsilon^2$, where ε is the ratio of the energy of the ν_τ to its maximum possible energy of 0.89 GeV (half the τ mass).
5. The production cross section of the F^+ F^- pair from proton-nucleus interactions had the form[8]

$$E\frac{d^3\sigma}{dp^3} \propto \frac{g(p_t,s)\,G(x)}{(\sqrt{p_t^2 + M_F^2} + 2.7)^{16.5}}$$

where

$$g(p_t,s) = \begin{cases} \exp(-1.06p_T), & \text{for } p_T < 1.0 \\ \exp\{(1-p_T)/\sqrt{s} - 1.06\}, & \text{for } p_T > 1.0 \end{cases}$$

$$G(x) = \begin{cases} 1, & \text{for } |x| < 0.25 \\ \left\{\frac{1-|x|}{0.75}\right\}^4, & \text{for } |x| > 0.25. \end{cases}$$

6. The integrated cross section of the F pair production per nucleon from 0 to 200 mrad in the laboratory system was 10 μb.

7. The cross section of the F pair production had the same A dependence as the proton absorption cross section; i.e. roughly proportional to $A^{2/3}$.

8. The lifetime of the F was so short that they decayed before being absorbed by beam dump material.

Figure 7 shows summed ν_τ flux and ν_τ fluxes for individual decay processes for the incident proton energy of 20 TeV. The detector radius was 0.5 m. Other decay modes of the τ (34%) which were not included in the calculations should yield τ neutrinos with slightly lower energies than those from the $\ell^- \bar{\nu}_\ell \nu_\tau$, $\pi^- \nu_\tau$ and $\rho^- \nu_\tau$ decays. Fluxes of τ antineutrinos are exactly the same as those of τ neutrinos. Figure 8 shows summed ν_τ fluxes for incident proton energies of 1, 5, 10, and 20 TeV.

Computed electron (or muon) neutrino (or antineutrino) fluxes from the $D(1.86) \rightarrow K(n\pi)\, e^+ \nu_e$ for the beam dump are shown in Figure 9 for incident proton energies of 1, 5, 10, and 20 TeV. The product of the $D\bar{D}$ production cross section and decay branching ratio into ν_e was assumed to be 10 μb. The energy spectrum of ν_e in the D rest frame was assumed to be the same as the measured electron spectrum from the D decay[9]. All the other conditions for the beam dump were the same as in the ν_τ case.

Table II gives computed event rates for a neutrino detector with the fiducial volume of 100 tons and the radius of 0.5 m. The total cross section of ν_τ and ν_e nucleon interactions was assumed to be $0.65 \cdot E_\nu$ (in GeV) x 10^{-38} cm^2. For 1 TeV the distance from the dump to detector was assumed to be 250 m.

The angular dependences of the ν_e and ν_τ fluxes are shown in Figure 10 for angular intervals of 0 to 0.5 mrad and 0.5 to 1.0 mrad. The incident proton energy was 20 TeV.

It must be noted that nuclear absorptions of F and D mesons in the dump are not neglibigle at higher energies. For example, if the lifetime of the F meson is 5×10^{-13} sec, the mean decay path of a 10 TeV F meson is 75 cm. Since the charm flavor is conserved in the absorption process, some fraction of absorbed F and D mesons will produce low energy neutrinos.

Since the production cross sections of charmed mesons are roughly proportional to A (instead of $A^{2/3}$), the neutrino fluxes shown in Figures 7 through 9 must be multiplied by $A^{1/3}$ where A is the atomic number of the dump material.

Muon neutrino and antineutrino fluxes from the pion and kaon decays in the beam dump have not been calculated in the present energy range. Contributions from secondary or tertiary or other higher order interactions have not been taken into account either. Detailed calculations of τ neutrino fluxes, and electron and muon neutrino fluxes from the beam dump including contributions from the pion and kaon decays were discussed in Reference 10 for the incident proton energies of 400 GeV and 1000 GeV.

An electron neutrino beam from the K_L^0 decay in the existing decay pipe at Fermilab has been studied for the incident proton energies of 400 GeV and 1000 GeV[11]. In the multi-TeV energy range it seems to be rather difficult to reduce $\bar{\nu}_\mu$ background from the $\Lambda^0 \rightarrow p\pi^- \rightarrow p\mu^-\bar{\nu}_\mu$ process because of the long lifetime of the Λ^0. Sweeping magnets will be required further downstream in the decay pipe. A beam dump can provide a high intensity electron neutrino and antineutrino beam with the $\nu_e^{(-)}/\nu_\mu^{(-)}$ ratio of 1[12]. It seems very attarctive at higher energies.

Counter experiments can tolerate relatively high muon backgrounds compared to bubble chamber experiments. In order to optimize the beam dump arrangement for both counter experiments and bubble chamber experiments a special arrangement such as shown below will be required.

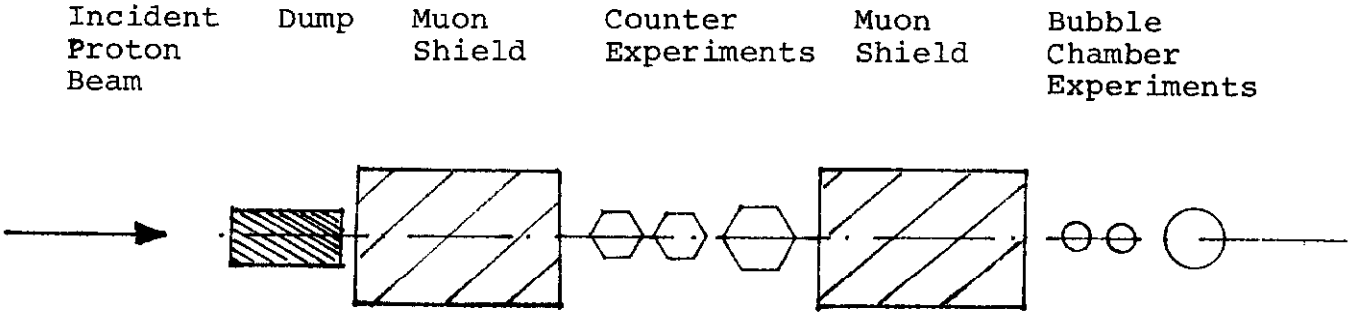

IV. Conclusions

Wide-band muon neutrino fluxes were computed for a bare target beam. For a detector with a small radius of about 0.25 m the decay path length of about 4 km can give a good flux even above 10 TeV. Low energy components can easily be suppressed. Enriched beams can be obtained. The muon shield length can be less than 2 km at the incident proton energy of 20 TeV. Elaborate focussing devices such as horns may not be needed. Arrangements of decay area and muon shield for the narrow-band beam will be totally different from those for the wide-band beam.

A beam dump can provide excellent electron neutrino and τ neutrino beams. Estimated ν_e and ν_τ event rates for a 100 ton detector with the radius of 0.5 m are $38 \times A^{1/3}$ and $1.2 \times A^{1/3}$, respectively, for 10^{13} incident protons at 20 TeV where A is the atomic number of the dump material. Since counter experiments can tolerate much higher muon backgrounds than bubble chamber experiments, a special arrangement will be desirable to give bubble chambers an additional muon shield.

Valuable discussions with G.Koizumi, A.Malensek, J.Peoples and the members of Working Group 6 of the second ICFA Workshop are greatly appreciated.

REFERENCES

1. G.Koizumi, "Muon dE/dx And Range Tables In The Multi-TeV Energy Range", Fermilab Internal Report TM-913, October 1979.

2. R.Adair and H.Kasha, Muon Physics, ed. by V.W.Hughes and C.S.Wu, (Academic Press, N.Y., 1977) Vol. 1, p. 324.

3. C.L.Wang, Phys. Rev. D7, 2609 (1973). Kaon production cross section was assumed to be 10% of pion production cross section.

4. See, for example, S.Mori et al., Phys. Rev. Letters 40, 432 (1978).

5. S.Mori, "Do We Need A Horn For Tevatron Neutrino Physics?", Fermilab Internal Report TM-839, December 1978.

6. There may be serious technical difficulties to build a horn system with a large $\int$ Bdl value.

7. J.Allaby et al., Fermilab 1976 Summer STudy Report, Vol. 2, p. 1.

8. I.Hinchliffe and C.H.Llewellyn Smith, Nucl. Phys. B114, 45 (1976), and M.Bourquin and J.M.Gaillard, Phys. Letters 58B, 191 (1976).

9. J.Kirkby, invited talk at Lepton-Photon Conference, Fermilab, August 1979.

10. S.Mori, "Estimated τ Neutrino Fluxes From A Beam Dump At 400 GeV And 1000 GeV", Fermilab Internal Report TM-848, January 1979.

11. S.Mori, "Improved Electron Neutrino Beam", Fermilab Internal Report TM-769, February 1978.

12. D.Cline, S.Mori, and R.Stefanski, "Neutrino Beam Dump Experiment And A Possible Electron Neutrino Beam In The Neutrino Area", Fermilab Internal Report TM-802, July 1978.

*Contributed paper to the Second ICFA Workshop

Table I. Computed event rates of a bare target beam for a 100 ton detector with the radius of 0.5 m and 10^{13} incident protons. The total cross section of ν_μ nucleon interactions was assumed to be 0.65 E_ν (in GeV) x 10^{-38} cm^2. The decay path length was 4 km and the muon shield length was 2 km. Wang's formula was used for particle production.

Incident Proton Energy (TeV)	Event Rate
1	5
5	140
10	400
20	740

Table II. Computed ν_τ and ν_e event rates for a beam dump for a 100 ton detector with the radius of 0.5 m and 10^{13} incident protons. The total cross section ν_τ and ν_e nucleon interactions was assumed to be 0.65 E (in GeV) x 10^{-38} cm^2. The distance between the beam dump and the detector was 1 km. We assumed that the cross section of the F pair production was 10 μb and that the product of the D pair production cross section and the branching ratio of the D decay into ν_e was 10 μb. We also assumed that cross sections of the charmed mesons are proportional to A where A is the atomic number of the dump material.

Incident Proton Energy (TeV)	Event Rate / $A^{1/3}$	
	ν_e	ν_τ
1	0.25	0.0086
5	1.9	0.059
10	11.3	0.34
20	38	1.2

FIGURE CAPTIONS

Figure 1. dE/dx curves of muons for soil, iron, and uranium. Solid curves correspond to energy losses due to atomic collision and pair production and dashed curves correspond to energy losses which include bremsstrahlung.

Figure 2. Range curves of muons for soil, iron, and uranium. Solid curves correspond to energy losses due to atomic collision and pair production and dashed curves correspong to energy losses which include bremsstrahlung.

Figure 3. Computed muon neutrino fluxes of the bare target beam for decay path lengths from 2 km to 20 km at the incident proton energy of 20 TeV. The detector radius was 0.5 m and the muon shield length was 2 km. Wang's formula was used for pion and kaon production.

Figure 4. Angular dependence of muon neutrino fluxes of the bare target beam for decay path lengths of 4 km and 10 km at the incident proton energy of 20 TeV.

Figure 5. Muon neutrino fluxes of the bare target beam at incident proton energies of 1, 5, 10, and 20 TeV for the decay path length of 4 km and the muon shield length of 2 km.

Figure 6. Muon neutrino fluxes as a function of a beam collimator aperture in a dog-leg arrangement. The detector radius was 0.5 m and the incident proton energy was 20 TeV.

Figure 7. Computed ν_τ fluxes for a beam dump at the incident proton energy of 20 TeV. The cross section for the F pair production was assumed to be 10 μb and proportional to $A^{2/3}$. The distance between the beam dump and the detector was 1 km. The detector radius was 0.5 m.

Figure 8. Computed ν_τ fluxes for a beam dump at incident proton energies of 1, 5, 10, and 20 TeV. The cross section for the F pair production was assumed to be 10 μb and proportional to $A^{2/3}$. The distance between the beam dump and the detector was 1 km. The detector radius was 0.5 m.

Figure 9. Computed electron (or muon) neutrino (or antineutrino) fluxes from the $D(1.86) \rightarrow K(n\pi)e^{+}\nu_e$ decay for a beam dump at incident proton energies of 1, 5, 10, 20 TeV. We assumed that $\sigma(D\bar{D})$ is proportional to $A^{2/3}$. The distance between the beam dump and the detector was 1 km. The detector radius was 0.5 m.

Figure 10. Angular dependence of electron neutrino and τ neutrino fluxes for a beam dump at the incident proton energy of 20 TeV. The distance between the beam dump and the detector was 1 km.

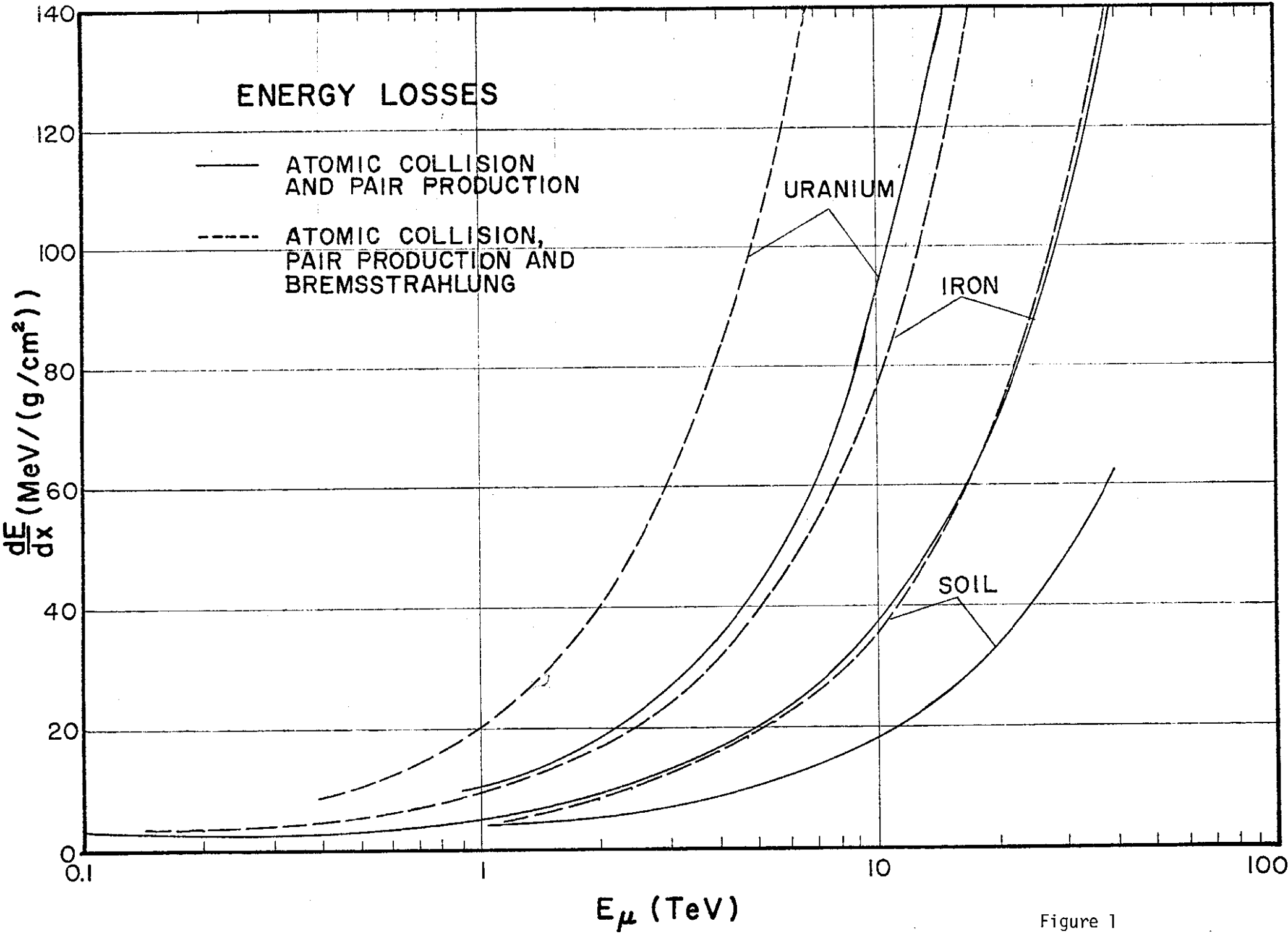
ENERGY LOSSES
ATOMIC COLLISION AND PAIR PRODUCTION
ATOMIC COLLISION, PAIR PRODUCTION AND BREMSSTRAHLUNG
URANIUM
IRON
SOIL
$\frac{dE}{dx}$ (MeV/(g/cm^2))
E_μ (TeV)
0
20
40
60
80
100
120
140
0.1
1
10
100

Figure 1

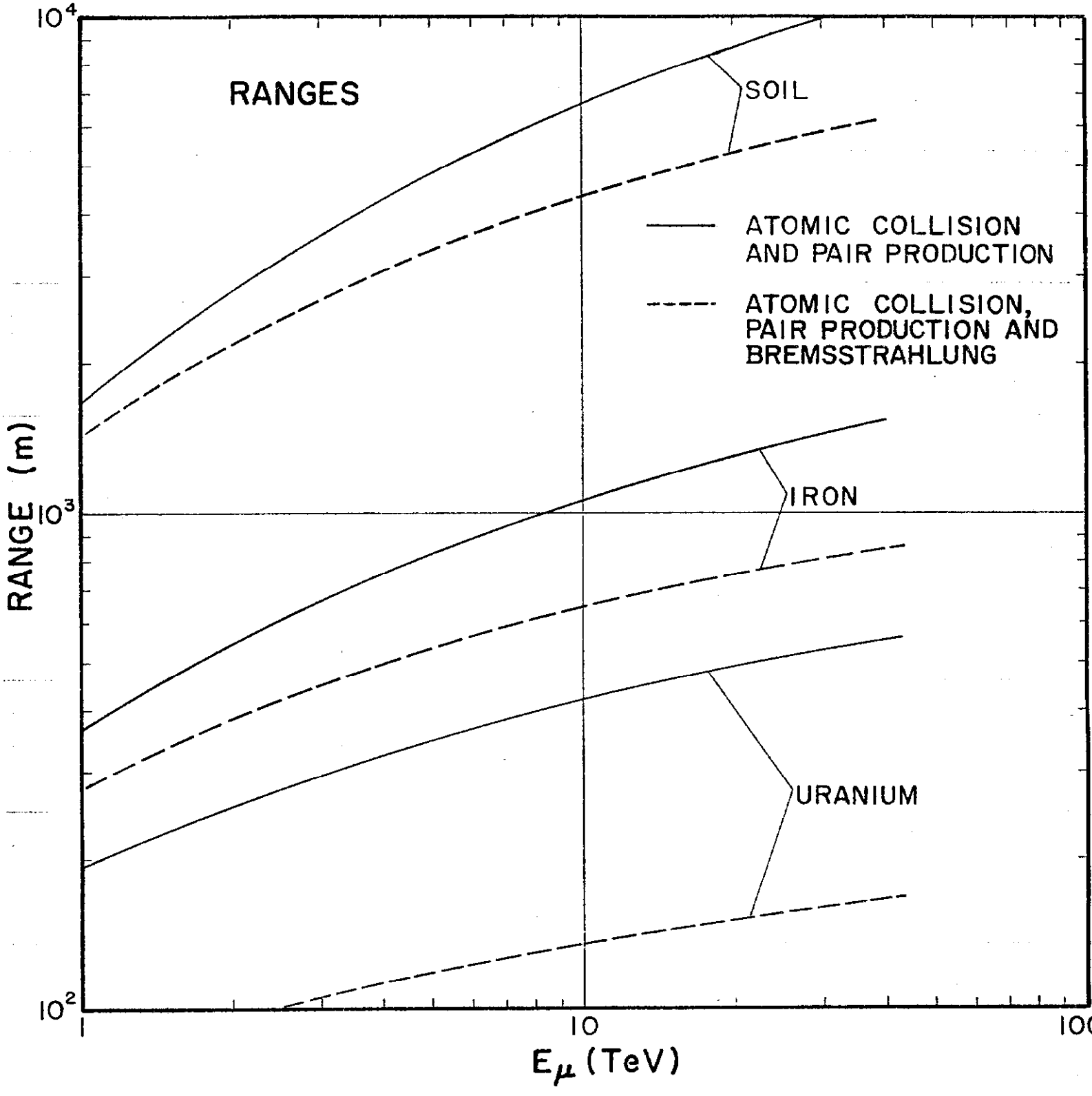
RANGES
SOIL
ATOMIC COLLISION AND PAIR PRODUCTION
ATOMIC COLLISION, PAIR PRODUCTION AND BREMSSTRAHLUNG
IRON
URANIUM
RANGE (m)
10^4
10^3
10^2
1
10
100
E_μ (TeV)

Figure 2

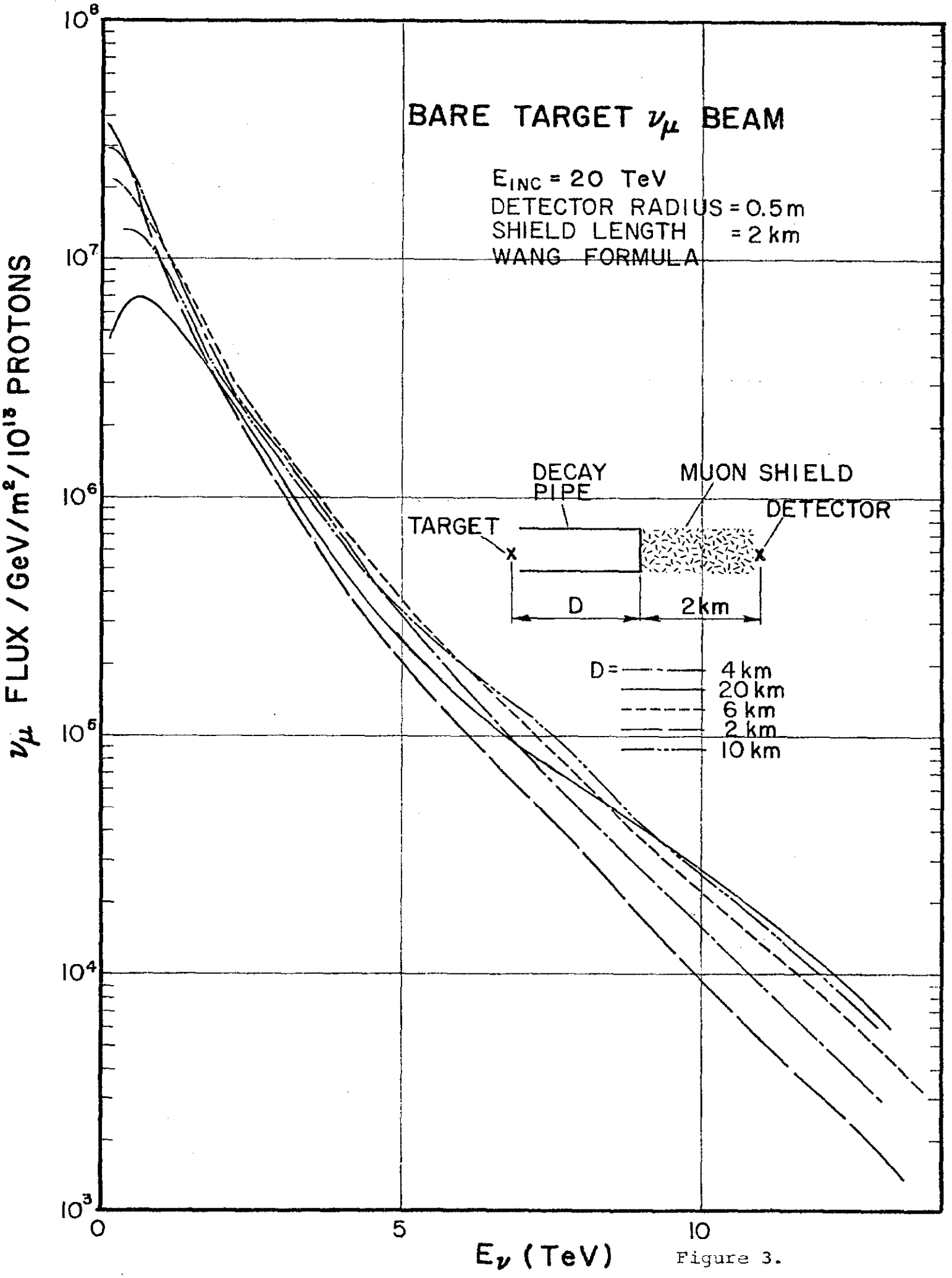
BARE TARGET ν_μ BEAM
E_{INC} = 20 TeV
DETECTOR RADIUS = 0.5m
SHIELD LENGTH = 2 km
WANG FORMULA
DECAY PIPE
MUON SHIELD
DETECTOR
TARGET
D
2km
D = 4 km
20 km
6 km
2 km
10 km
ν_μ FLUX / GeV/m^2/10^{13} PROTONS
E_ν (TeV)
10^8
10^7
10^6
10^5
10^4
10^3
0
5
10

Figure 3.

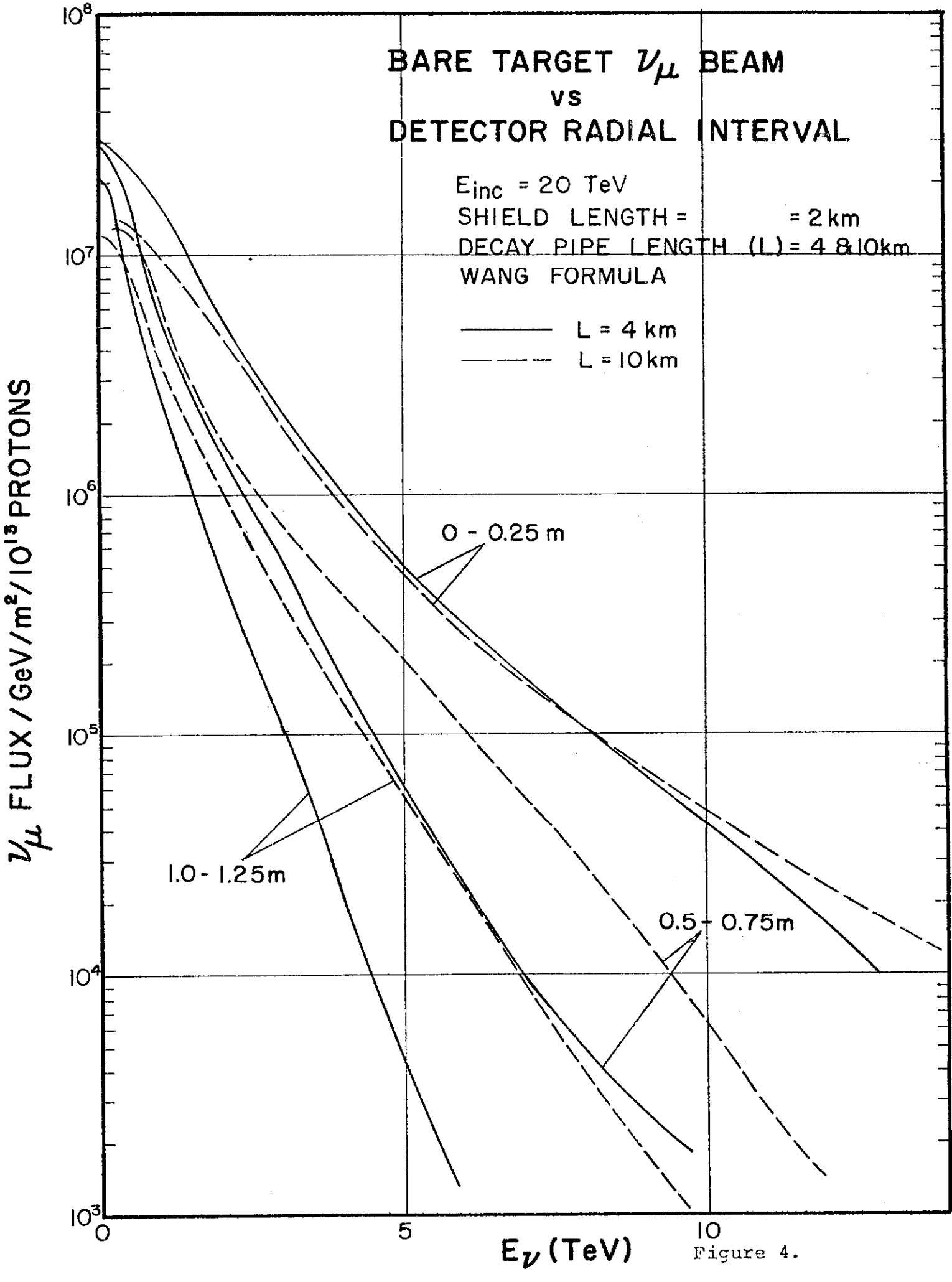
BARE TARGET ν_μ BEAM
vs
DETECTOR RADIAL INTERVAL
E_{inc} = 20 TeV
SHIELD LENGTH = = 2 km
DECAY PIPE LENGTH (L) = 4 & 10km
WANG FORMULA
L = 4 km
L = 10km
0 - 0.25 m
1.0 - 1.25m
0.5 - 0.75m
ν_μ FLUX / GeV/m^2/10^{13} PROTONS
E_ν (TeV)
10^8
10^7
10^6
10^5
10^4
10^3
0
5
10

Figure 4.

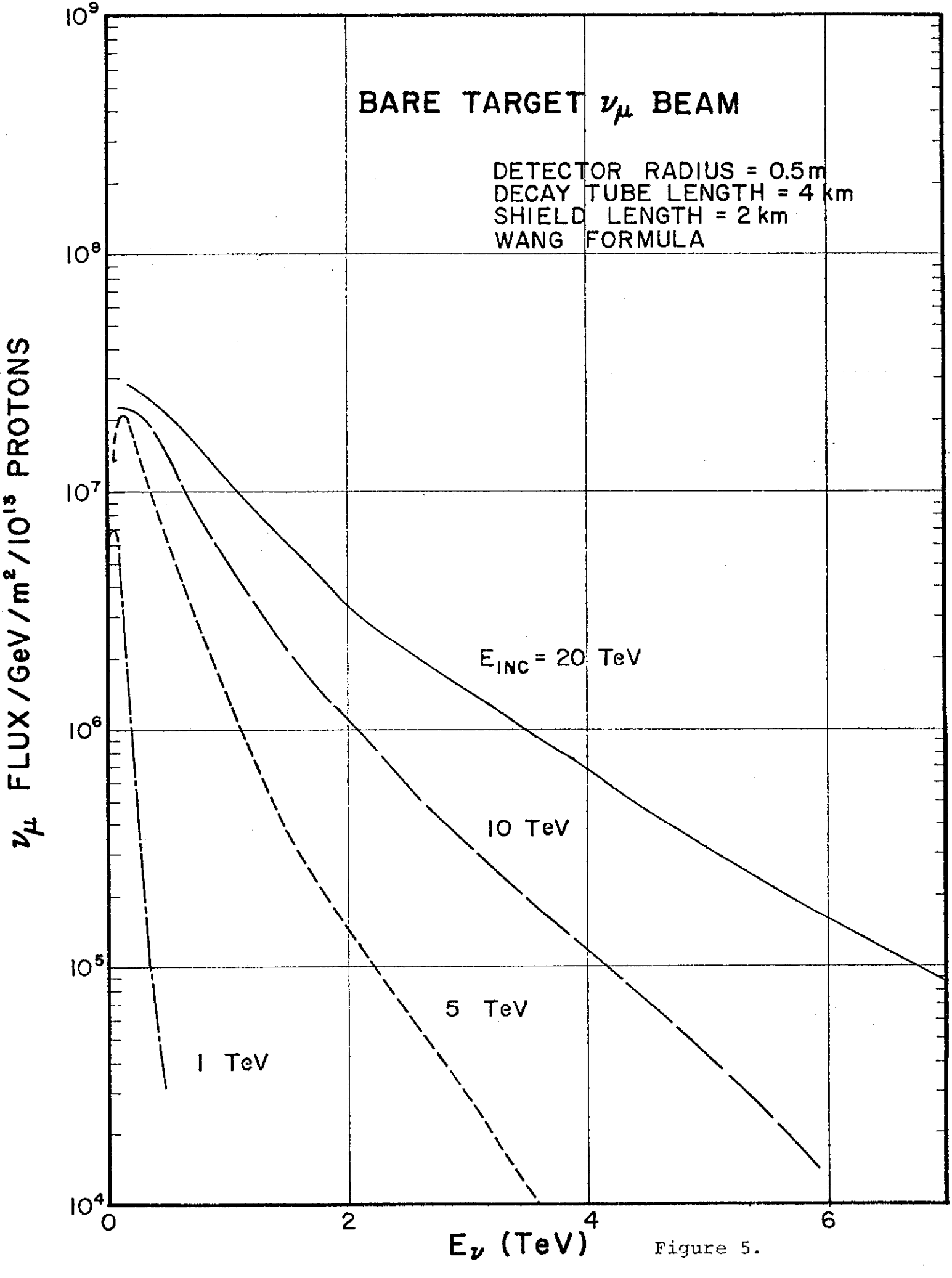
BARE TARGET ν_μ BEAM
DETECTOR RADIUS = 0.5m
DECAY TUBE LENGTH = 4 km
SHIELD LENGTH = 2 km
WANG FORMULA
E_{INC} = 20 TeV
10 TeV
5 TeV
1 TeV
ν_μ FLUX / GeV / m^2 / 10^{13} PROTONS
E_ν (TeV)
10^9
10^8
10^7
10^6
10^5
10^4
0
2
4
6

Figure 5.

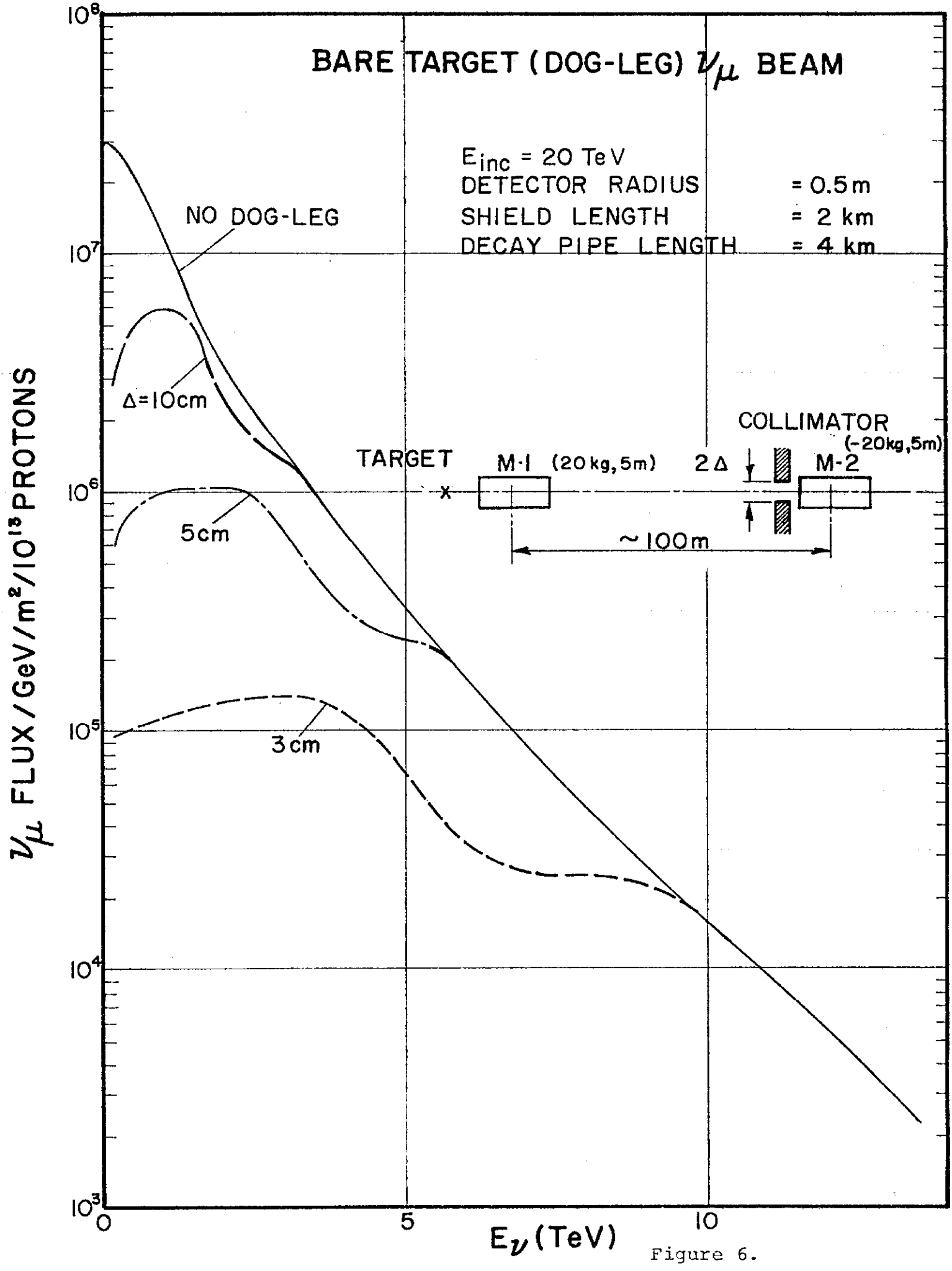
BARE TARGET (DOG-LEG) ν_μ BEAM
E_{inc} = 20 TeV
DETECTOR RADIUS = 0.5m
SHIELD LENGTH = 2 km
DECAY PIPE LENGTH = 4 km
NO DOG-LEG
Δ=10cm
5cm
3cm
TARGET
M-1 (20kg, 5m)
2Δ
COLLIMATOR
(-20kg, 5m)
M-2
~100m
ν_μ FLUX / GeV / m^2 / 10^{13} PROTONS
10^8
10^7
10^6
10^5
10^4
10^3
0
5
10
E_ν (TeV)

Figure 6.

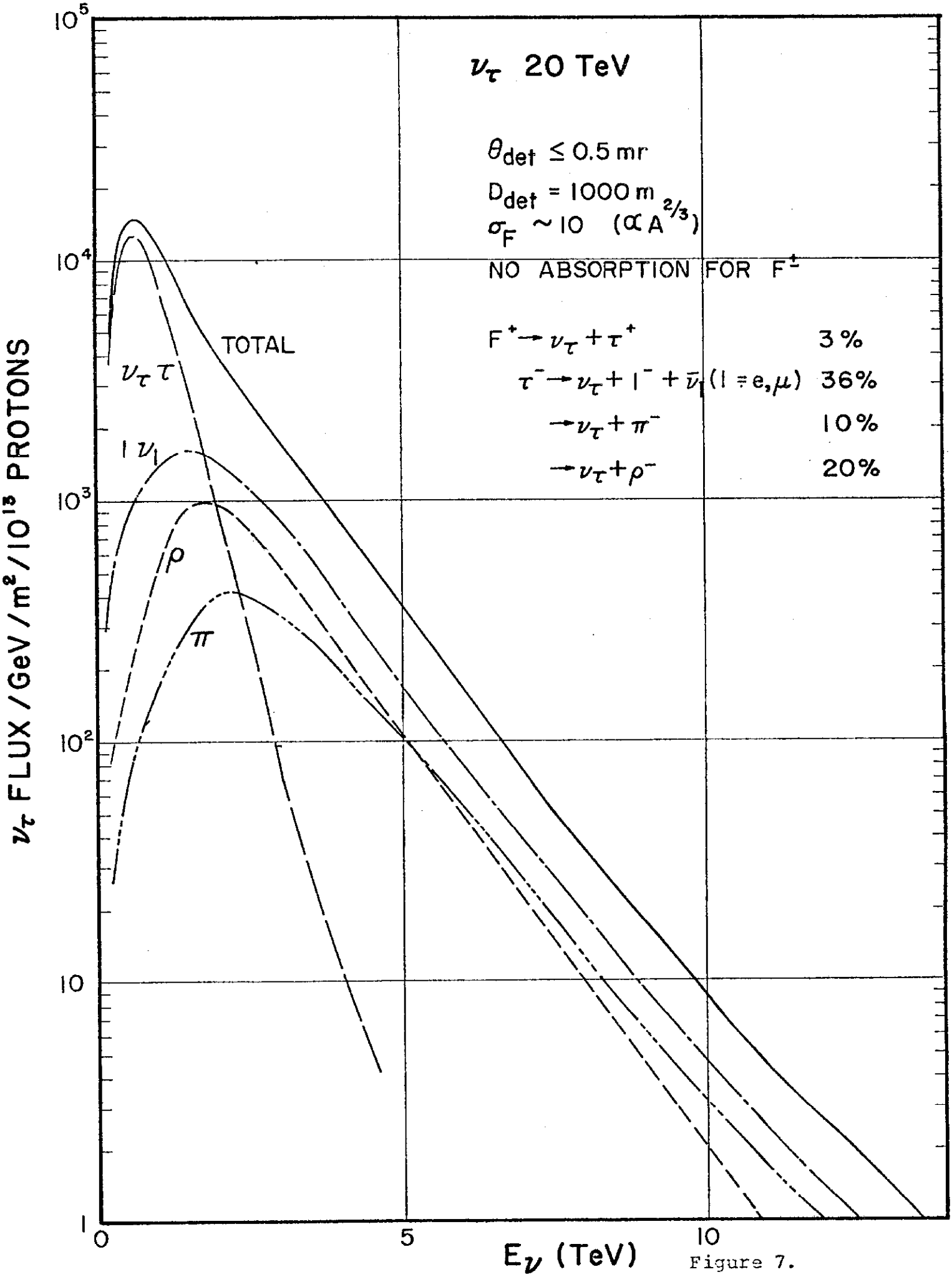
ν_τ 20 TeV
$\theta_{det} \leq 0.5$ mr
$D_{det} = 1000$ m
$\sigma_F \sim 10 \quad (\propto A^{2/3})$
NO ABSORPTION FOR $F^{\pm}$
$F^+ \rightarrow \nu_\tau + \tau^+$ 3 %
$\tau^- \rightarrow \nu_\tau + l^- + \bar{\nu}_l \; (l = e, \mu)$ 36 %
$\rightarrow \nu_\tau + \pi^-$ 10 %
$\rightarrow \nu_\tau + \rho^-$ 20 %
TOTAL
$\nu_\tau \tau$
$l \nu_l$
ρ
π
10^5
10^4
10^3
10^2
10
1
0
5
10
E_ν (TeV)
ν_τ FLUX /GeV /m^2 /10^{13} PROTONS

Figure 7.

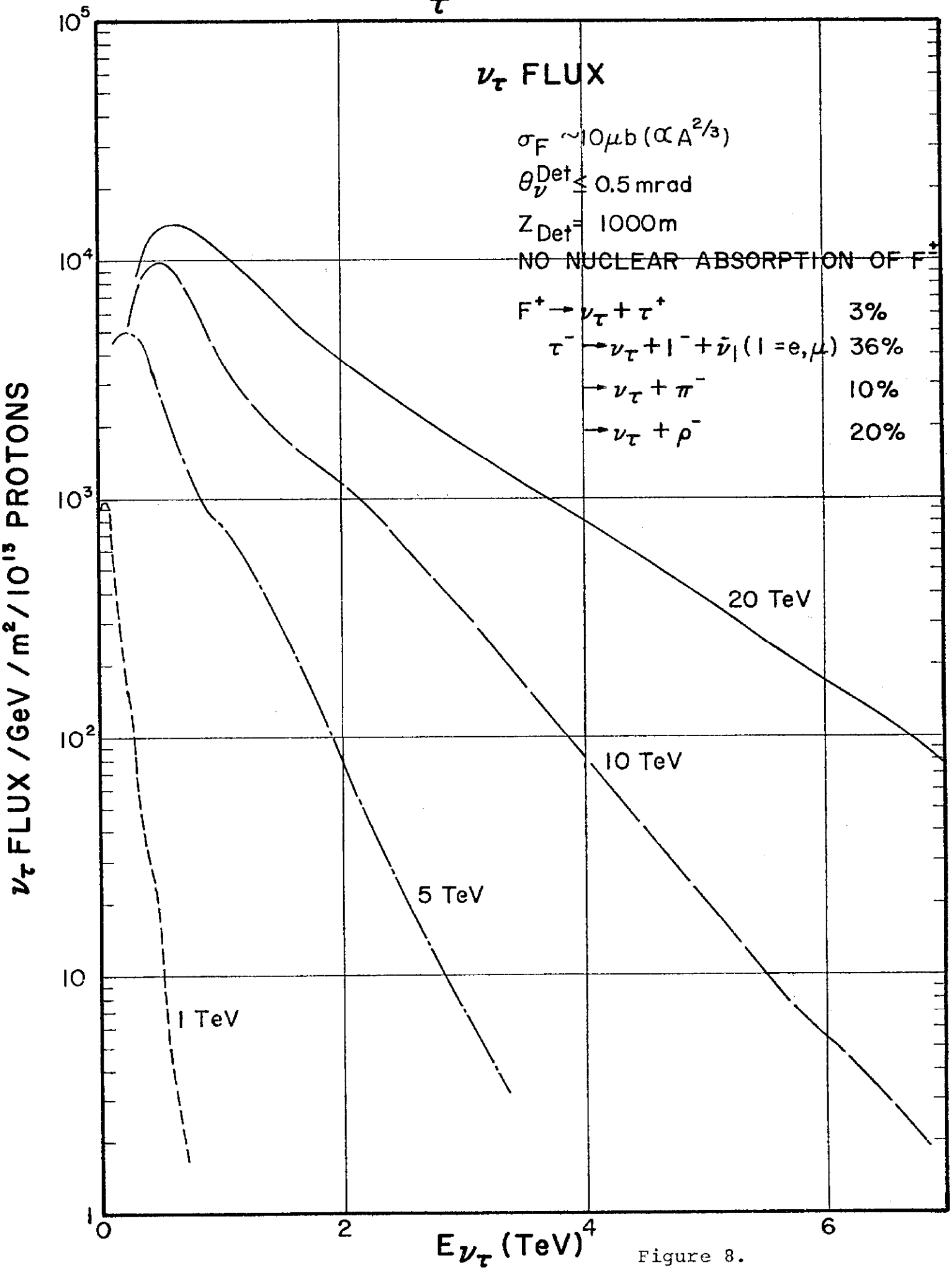
ν_τ FLUX
$\sigma_F \sim 10\mu b\ (\propto A^{2/3})$
$\theta_\nu^{Det} \leq 0.5$ mrad
$Z_{Det} = 1000$m
NO NUCLEAR ABSORPTION OF $F^{\pm}$
$F^+ \rightarrow \nu_\tau + \tau^+$ 3%
$\tau^- \rightarrow \nu_\tau + l^- + \bar{\nu}_l\ (l = e, \mu)$ 36%
$\rightarrow \nu_\tau + \pi^-$ 10%
$\rightarrow \nu_\tau + \rho^-$ 20%
20 TeV
10 TeV
5 TeV
1 TeV
ν_τ FLUX /GeV /m^2/10^{13} PROTONS
E_{ν_τ} (TeV)
10^5
10^4
10^3
10^2
10
1
0
2
4
6

Figure 8.

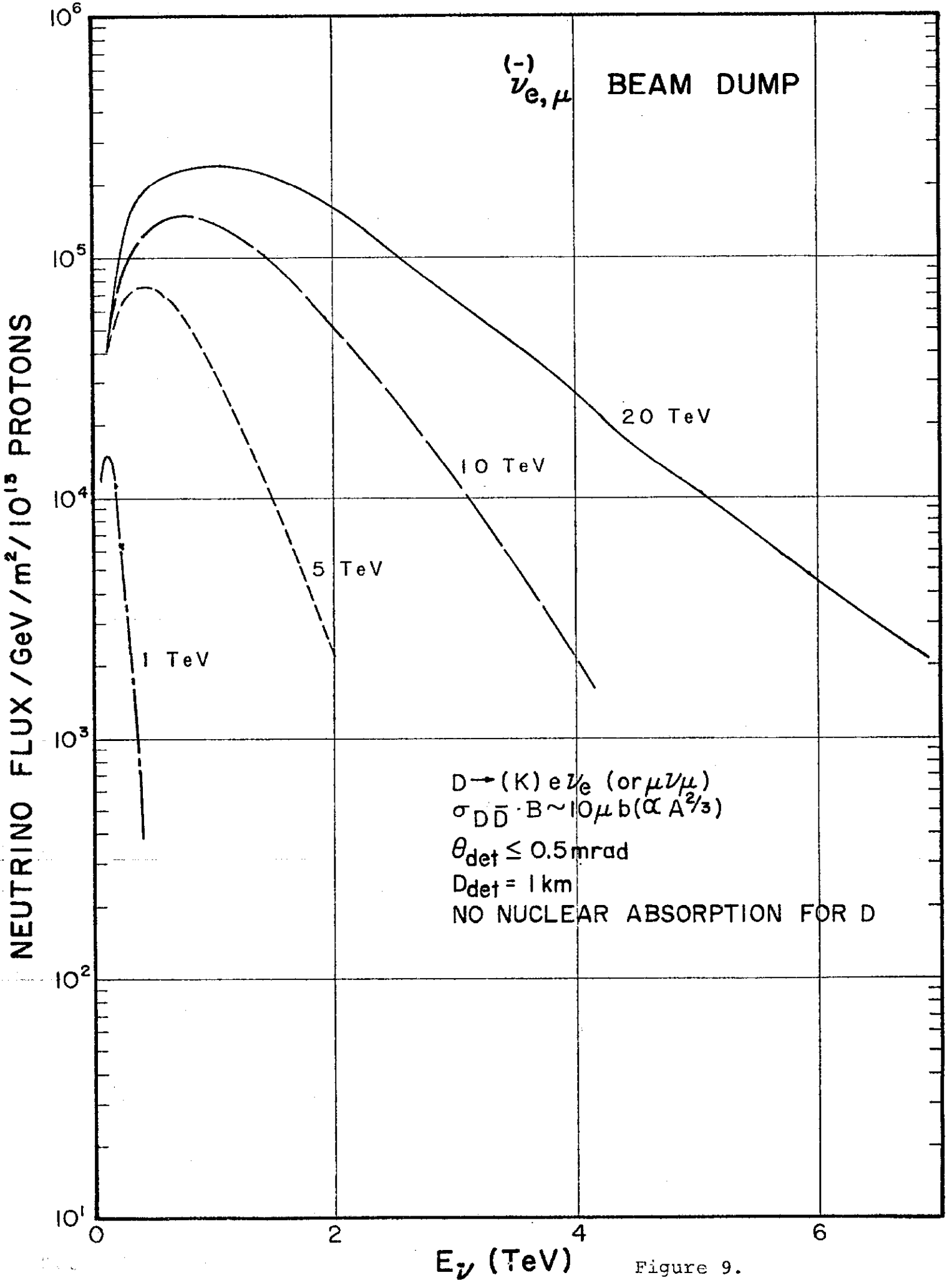
$\overset{(-)}{\nu}_{e,\mu}$ BEAM DUMP
20 TeV
10 TeV
5 TeV
1 TeV
D → (K) e ν_e (or $\mu\nu_\mu$)
$\sigma_{D\bar{D}} \cdot B \sim 10\mu b (\propto A^{2/3})$
$\theta_{det} \leq 0.5$ mrad
$D_{det} = 1$ km
NO NUCLEAR ABSORPTION FOR D
NEUTRINO FLUX / GeV / m² / 10^{13} PROTONS
E_ν (TeV)
10^6
10^5
10^4
10^3
10^2
10^1
0
2
4
6

Figure 9.

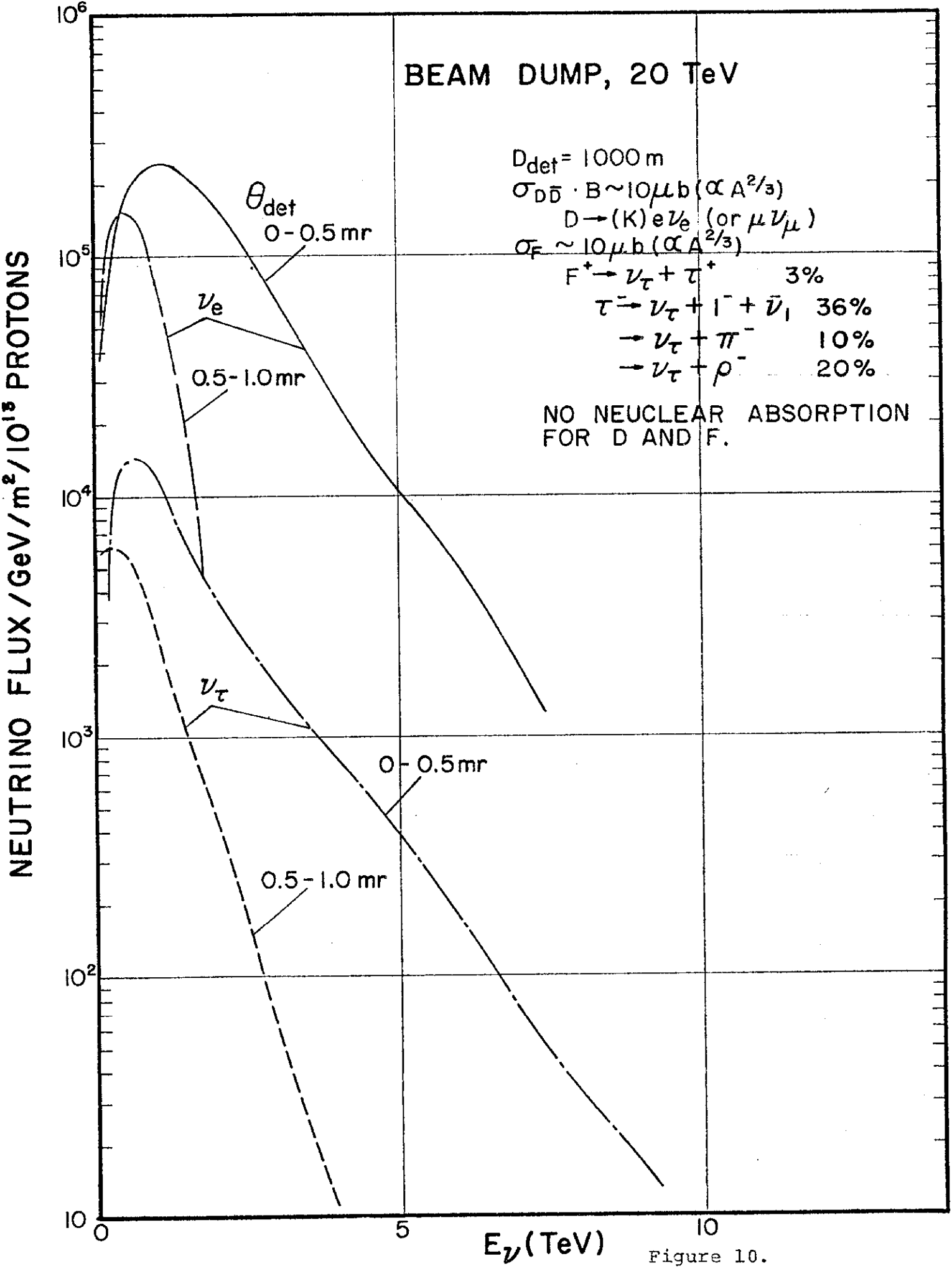
BEAM DUMP, 20 TeV
D_{det} = 1000 m
$\sigma_{D\bar{D}} \cdot B \sim 10\mu b (\propto A^{2/3})$
$D \rightarrow (K) e \nu_e$ (or $\mu \nu_\mu$)
$\sigma_F \sim 10\mu b (\propto A^{2/3})$
$F^+ \rightarrow \nu_\tau + \tau^+$ 3%
$\tau^- \rightarrow \nu_\tau + l^- + \bar{\nu}_l$ 36%
$\rightarrow \nu_\tau + \pi^-$ 10%
$\rightarrow \nu_\tau + \rho^-$ 20%
NO NEUCLEAR ABSORPTION FOR D AND F.
θ_{det}
0 - 0.5 mr
ν_e
0.5 - 1.0 mr
ν_τ
0 - 0.5 mr
0.5 - 1.0 mr
NEUTRINO FLUX / GeV / m^2 / 10^{13} PROTONS
10^6
10^5
10^4
10^3
10^2
10
0
5
10
E_ν (TeV)

Figure 10.